BIBECHANA
Vol. 22, No. 3, December 2025, 237-247

ISSN 2091-0762 (Print), 2382-5340 (Online)
Journal homepage: http://nepjol.info/index.php/BIBECHANA
Publisher:Dept. of Phys., Mahendra Morang A. M. Campus (Tribhuvan University)Biratnagar

Exploring the structural, mechanical, dynamical, thermal, electronic, magnetic, and optical properties of monolayer WTe_2 compound: First-principles study

Sukrit Kumar Yadav, Tejendra Neupane, Arpan Pokharel, Kamal Khanal, Karan Deuba, Om Shree Rijal, Hari Krishna Neupane*

Amrit Campus, Institute of Science and Technology, Tribhuvan University, Kathmandu Nepal

*Corresponding author. Email: hari.neupane@ac.tu.edu.np

Abstract

The potential applications of materials are determined by their existing properties. In this work, we used first-principles approach to investigate the structural, mechanical, dynamical, thermal, electronic, magnetic, and optical properties of (3×3) supercell structure of Tungsten ditelluride (WTe_2) compound using GGA-PBE functional of density functional theory (DFT) method. Structural properties of WTe_2 compound are studied by measuring bond lengths between the atoms in structure, and ground state energy. It is found to be structurally stable material. Electronic band structure and density of states (DOS) plot shows that the material has direct band gap p-type semiconductor. Magnetic properties of WTe_2 compound are predicted by the analysis of its density of states (DOS) and partial density of states (PDOS) plots, material is found to be non-magnetic in nature. The mechanical properties of considered compound are examined by the calculations of its modulus of rigidities, elastic constants, elasticity and anisotropy index. WTe_2 has ductile and anisotropic properties. Moreover, we have examined the dynamical stability of considered material through the phonon dispersion curve, it reveals that WTe_2 is dynamically stable material. Based on the calculations of phonon velocities and Debye temperature, it is found that WTe_2 has low value of specific heat capacity. Dielectric function, optical conductivity, absorption, transmission, and reflection coefficients of WTe_2 compound are examined for the exploration of its optical characteristics. At higher photon energy region, WTe_2 has transparent and anisotropic in nature, higher value of conductivity, lower values of absorption and reflection coefficient. Hence, it can be used in the fields of electronic, optoelectronic, sensing, and energy storage devices.

Keywords
Dynamical, electronic, magnetic, mechanical, optical, thermal.

Article information
Manuscript received: March 5, 2025; Revised: June 20, 2025; Accepted: August 4, 2025
DOI https://doi.org/10.3126/bibechana.v22i3.76349

1 Introduction

Two-dimensional (2D) materials are made up of a single or few layers of having a thickness of a few nanometers or less [1,2]. Graphene, transition-metal dichalcogenides (TMDCs) materials, hexagonal boron nitride (h-BN) etc. are the common examples of 2D materials [3–5]. TMDCs materials are the types of 2D materials having a structure of the form MX_2, where M represents transition metals from group IV-X (W or Mo), and X represents Chalcogens material (Te, S, or Se) [6]. M is sandwiched between two layers of X atoms by forming the X-M-X honeycomb pattern [7]. There is a strong covalent bond between the atoms in each layer, but the layers are stacked together by weak van der Waals forces [8]. TMDCs pose exceptional catalytic [9], photoluminescence [10] direct band gap, and water resistance properties [11]. So, they are used in the field of electronics and nanoelectronics for making devices such as transistors, integrated circuits (ICs), and memory devices [9, 10]. They are used in flexible and wearable electronics, spintronics, quantum computing, and spin hall effect devices [12]. Similarly, they are used in energy storage devices like batteries and capacitors, hydrogen evolution reactions, electrocatalysis, gas sensors, biosensors, thermoelectric devices, water purification technologies, and solid lubricants [13]. TMDCs are used in optoelectronic devices and photo detectors due to its tunable band structure [14, 15]. Thus, 2D materials have potential applications in the fields of industrial as well as academic sectors.

We have reviewed the various literature related with the TMDCs materials [16,17] it is found that bulk WTe_2 has large magnetoresistance and finds application in magnetic sensors and memory devices. To our best knowledge, a comprehensive study of structural, mechanical, dynamical, thermal, electronic, magnetic, and optical properties of monolayer WTe_2 TMDCs material have not been studied well. These are the research gaps between the previous researcher's works and our work. The tunability of these properties of TMDCs has made them a topic of great research. So, we are motivated to explore the structural, mechanical, dynamical, thermal, electronic, magnetic, and optical properties of (3×3) monolayer supercell structure of 2D WTe_2 TMDCs compound computationally by using Density Functional Theory (DFT) method employing quantum ESPRESSO as a computational tool.

2 Methods and Material

First-principles calculations based on plane wave function and ultrasoft pseudopotentials (USPPs) are performed using the density functional theory (DFT) technique by employing the Quantum ESPRESSO as a computational tool [17]. To handle the exchange-correlation interactions, we employed the generalized gradient approximation (GGA) in Perdew-Burke-Ernzerhof (PBE) form [18,19]. Firstly, we have constructed the optimized and relaxed unit cell structure of WTe_2 material by using the optimized values of lattice parameter 12 Bohr (6.35 Å), kinetic energy cutoff 45 Ry (612.25 eV), and k-points (12) through Broyden–Fletcher–Goldfarb–Shanno (BFGS) method [20]. The k-point grid of mesh (12×12×1) is used to sample Brillouin zone by using -centered Monkhorst–Pack (MP). The optimized and relax structure unit cell structure of WTe_2 is extended three times along x-and y-directions to form (3×3×1) monolayer supercell structure of WTe_2. Then after relax calculations are done by using Broyden–Fletcher–Goldfarb–Shanno (BFGS) method [20], which gives the optimized and relax supercell structure of WTe_2. This structure is used for further calculations. The structural properties of considered material are studied by the calculations of its ground state energy through self-consistent field (scf) calculations where (12×12×1) k-point mesh is used. For the study of material's electronic and magnetic properties, band structure, density of states (DOS) and partial density of states (PDOS) calculations are done. For this denser mesh (22×22×1) is used since denser mesh gives the smoother DOS states. The mechanical and thermal properties of material are examined by the calculations of its modulus of rigidity and elastic constants through Voigt-Reuss-Hill approach [21]. Based on the computed values of elastic constants, we have estimated the Shear modulus (G), Bulk modulus (B), Young's modulus (E), Poisson's ratio (v), Pugh's ratio (B/G), Debye temperature ($_D$), Longitudinal phonon wave velocity (v_l), transverse phonon wave velocity (v_t), and average phonon wave velocity (v_{avg}). Additionally, density functional perturbation theory (DFPT) techniques are used to analyze the dynamical properties of the materials under consideration [22]. The optical properties of WTe_2 compound are studied by calculating it dielectric function, optical conductivity, transmission, reflection and absorption coefficient through the uses of time-dependent ground state perturbation theory under random phase approximation (RPA) [23].

3 Results and Discussion

In this section, we have discussed the major findings and their interpretation of (3×3) monolayer supercell structure of 2D WTe_2 TMDCs compound.

3.1 Structural Properties

The structural properties of WTe_2 unit cell compound are studied by calculating its optimized values of kinetic energy cutoff, lattice parameters, and k-points. They are found to be 45 Ry, 6.35 Å, and 12 respectively. Then, relax calculations are done by using (12×12×1) k-point mesh. The relax and optimized unit cell structure is extended along x-and y-axis by three times to construct its (3×3) supercell structure. The ground state energy of supercell structure is estimated through its self-consistent fields (scf) calculations, and found to be -238.10 eV. This minimum value of ground state energy revels that WTe_2 is a stable material. The optimized and relax structure of WTe_2 supercell is shown in figure-1(a & b).

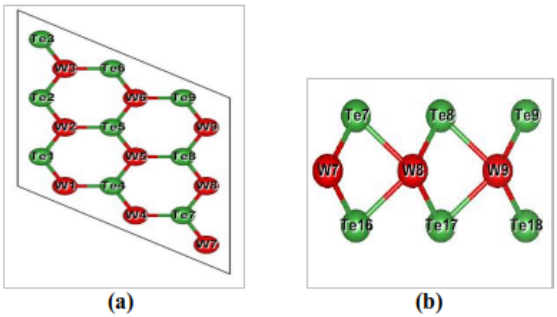

Figure 1: (Colour Online) (a) top view of (3×3) supercell structure of WTe_2 compound (b) side view of (3×3) supercell structure of WTe_2 compound.

Table 1: Inter-atomic distance between W-W, W-Te, and Te-Te before and after relaxation compared with previously reported values.

Bond length	Before relaxation (Å)	After relaxation (Å)	Reported values (Å)
W–W	3.57	3.32	3.55
W–Te	2.73	2.53	2.73
Te–Te	3.57	3.23	[24]

Figure-1(a) is the top view of the monolayer WTe_2 supercell compound from z-axis. The unit cell is hexagonal structure with alternating W and Te atoms arranged in hexagonal shape. Figure-1(b) shows the side view (i.e. x-axis or y-axis) of WTe_2 supercell material. In this view, the layer of W is sandwiched between two Te layers. Table-1 summarizes the bond lengths before and after the relaxation of a considered compound. Before relaxation, the inter-atomic distance between adjacent W-W, W-Te, and Te-Te atoms are found to be 3.57 Å, 2.73 Å, and 3.57 Å respectively. Whereas after relaxation the inter-atomic distance reduces to 3.32 Å, 2.53 Å, and 3.23 Å respectively of these atoms in a structure. These values are closely agreed with the previously reported values of stable TMDCs materials [24]. Hence, from these calculations, we confirmed that our considered material is a structurally stable.

3.2 Mechanical, Dynamical and Thermal Properties

Mechanical behavior of WTe_2 compound such as stiffness, deformation response, and stability under different external loads are determined by the measurement of parameters like elastic constants and modulus of rigidities (Young's modulus, Shear modulus, Bulk modulus), and compressibility (β). Approximations like Voigt (V) [25], Reuss (R) [26], and Hill [27] are used to calculate these mechanical parameters. The Voigt model assumed uniform strain throughout crystal and calculated the upper bound of the elastic moduli whereas Reuss model assumed a uniform stress across the material and calculated the lower bound of the elastic moduli. Hill model calculated the parameters by averaging the results obtained from formed two models. The Bulk modulus (B) measures the material's resistance to uniform compression. In case of hexagonal system, it is determined by averaging the Bulk modulus of elasticity from the Voigt (B_V) and Reuss (B_R) models and given by;

$$B_H = \frac{1}{2}\left(B_v + B_R\right) \tag{1}$$

The Shear modulus (S_H) measures the material's resistance to shearing forces. It is determined by averaging the Shear modulus from the Voigt (S_R) models;

$$S_H = \left(S_V + S_R\right) \tag{2}$$

For hexagonal crystal systems, the Voigt approximations for the Bulk modulus B_V and Shear modulus S_V are expressed as;

$$B_V = \frac{1}{9}\left[2\left(C_{11} + C_{12}\right) + 4C_{13} + C_{33}\right] \tag{3}$$

$$S_v = \frac{1}{30}\Big[\left(C_{11} + C_{12}\right) + 2C_{33} - 4C_{13} + 12C_{44} + 12C_{66}\Big] \tag{4}$$

For the Reuss approximation, the Bulk modulus B_R and Shear modulus S_R are defined as;

$$B_R = \frac{(C_{11}+C_{12})C_{33}-2C_{13}^2}{C_{11}+C_{12}+2C_{33}-4C_{13}} \quad (5)$$

$$S_R = \frac{5}{2}\frac{(C_{11}+C_{12})C_{33}-2C_{13}^2}{\left[3B_vC_{55}C_{66}+(C_{11}+C_{12})C_{33}-2C_{13}^2\right]^2(C_{55}+C_{66})} \quad (6)$$

The compressibility (β) measures how much the material's volume changes under pressure and it is given by the inverse of the Bulk modulus (B) i.e. $\beta = 1/B$. For pristine WTe_2, Young's modulus (Y) is an important mechanical property that indicates the material's stiffness or rigidity. It measures how much WTe_2 deforms under stress, providing insight into its ability to resist elastic deformation. A higher Young's modulus means that WTe_2 is stiffer and deforms less under a given load. Young's modulus can be determined using the Hill approximation, which is approximate for polycrystalline materials like WTe_2. The formula for Young's modulus is;

$$Y = \frac{9B_HS_H}{3B_H+S_H} \quad (7)$$

where B_H is the Hill Bulk modulus, which quantifies WTe_2's resistance to uniform compression and S_H is the Hill Shear modulus, which describes WTe_2's resistance to shearing forces. By applying this formula, we can accurately assess how the pristine WTe_2 will behave under mechanical stress. For WTe_2, elastic anisotropy (A) measures the variation in stiffness with direction.

It reflects how mechanical properties like stiffness and deformation change depending on the direction of applied force. High anisotropy (A) means WTe_2 behaves differently along different crystallographic directions. For hexagonal systems, it is expressed as [28];

$$A = \frac{4C_{44}}{C_{11}+C_{33}-2C_{13}} \quad (8)$$

Poisson's ratio (ν) is calculated using an equation (9);

$$\nu = \frac{3B-2S_H}{2(3B+S_H)} \quad (9)$$

The calculated values of various parameters for the examination of mechanical properties are mentioned in the Table-2.

Table 2: Estimated values of Bulk modulus (B), Young's modulus (Y), Shear modulus (G), Poisson's ratio (ν), P-wave modulus, and Pugh's ratio (B/G) of WTe_2 compound.

Mechanical Properties	**Voigt**	**Reuss**	**Hill**
Bulk Modulus B (GPa)	14.78	-0.73	7.03
Young's Modulus Y (GPa)	24.74	-2.57	10.85
Shear Modulus G (GPa)	10.13	-1.40	4.37
Poisson's Ratio (ν)	0.22	-0.08	0.24
P-wave Modulus (GPa)	28.29	-2.60	12.85
Pugh's Ratio (B/G)	1.46	0.52	1.61

The Bulk modulus (B) of WTe_2 is found to be 7.03 GPa which indicates that it requires 7.03 GPa to uniformly compress its volume by 1%. Hence, it is relatively compressible compared to other materials like diamond [29]. The Young's modulus (Y) of WTe_2 is 10.85 GPa means that it is relatively flexible as compared to the material with higher Young's modulus such as steel [30]. The Shear modulus (G) of WTe_2 is calculated as 4.37 GPa indicates that it is relatively soft in the resistance compared to the material like steel which has Shear modulus of 80 GPa. A Poisson's ratio (ν) of WTe_2 is found to be 0.24, which indicates that the contraction in perpendicular direction at 24.3% of the rate of elongation when stretched out in one direction. This is moderate value. It has a P-wave modulus 12.85 GPa, which means that it can efficiently transmit compressional waves. The Pugh's ratio (B/G) of WTe_2 material is found to be 1.61, it suggests that the material is relatively ductile [31–33]. Furthermore, the Kleinman's parameter is calculated to be 0.45 which is less than the reference value 0.5 that determines the type of deformations when external perturbations are applied. Thus, it suggests that bond bending is more dominant than bond stretching [31–33].

The dynamical properties (stability) of the material are determined by studying its phonon dispersion curve. Phonon dispersion curve measures how the phonon frequencies (measured in terms of wavenumber) vary with wave vectors across the Brillouin zone [34]. Figure-2 shows the phonon

dispersion curve of WTe_2 compound, where wave numbers (frequency) are plotted along y-axis and wave vectors (symmetric points) are along x-axis. The graph does not show any negative wavenumber which indicates the absence of negative frequency. Thus, the material is found to be dynamically stable. The lower three bands are for acoustic phonons whereas the upper six bands are for optical phonons. The acoustic phonons at the center of Brillouin zone (i.e. Γ point) have zero frequencies. But the optical phonons have non-zero frequencies and are found to be 3.55, 5.27, 5.76, and 7.16 in units of per centimeters. The above results are consistent with previous studies [35,36]. It is seen that there is phonon band gap energy of values 0.30 per centimeter, which is calculated from the lower position of optical branches and upper position of the acoustical branches.

Moreover, we have investigated the thermal properties of WTe_2 compound by estimated its phonon velocities and Debye temperature. For that we have estimated the longitudinal velocity, transverse velocity and average velocity of phonon wave of WTe_2 material. They are found to be 1665.76 m/s, 971.05 m/s, and 1077.12 m/s respectively. We have estimated the Debye temperature of WTe_2 material, and found to be 85.6 K. It reflects that WTe_2 has a low melting point and has low value of specific heat capacity.

3.3 Electronic and Magnetic Properties

The wave functions that describe the electrons in solid can be studied by sampling on the Brillouin zone (BZ). Highly symmetric points in the BZ are used to study the material's band structure. In the present work, we have studied the electronic properties of pristine WTe_2 compound with the help of band structure and density of states (DOS) plots. Figure-3(a & b) respectively represent the band structure and DOS plots of considered material, where the horizontal dot line indicates the Fermi energy level. It separates the electronic bands. The region below the Fermi line is called valence band, and above the Fermi line is called conduction band.

Figure-3(a) is the band structure of WTe_2 compound with high symmetric points are in the x-axis and Fermi energy level is adjusted in the unit of eV along y-axis. The blue dashed line set at 0 eV is the Fermi energy level. The plots in red lines (states) represent the band states of the electrons located at different points in Brillouin zone. The region below the Fermi level are valence bands, and the region above the Fermi level are conduction bands. The plot shows a clear gap between the valence band maxima and conduction band minima. Thus, monolayer WTe_2 shows semiconductor nature. From the calculations, the value of conduction band minimum (CBM) is found to be 0.95 eV, and the valence band maximum (VBM) is 0.04 eV both lying at symmetric points. Thus, the band gap, defined as the gap between VBM and CBM, is calculated to be 0.99 eV. This value is consistent with previous reported values of materials that is in the range of (0.70 -1.18) eV. This material has direct band gap energy because CBM and VBM both lie at point which signifies that the inter-band transition of electrons happened without change in momentum. The valence band is closer to Fermi level than the conduction band, this suggests the higher probability of finding holes in the valence band and material shows p-type semiconductor behavior. Finally, we can conclude that pristine monolayer WTe_2 is a p-type and direct band gap semiconductor, and thus it has potential applications in semiconductor industries.

Table 3: Valence band maximum (VBM), conduction band minimum (CBM), band gap energy (E_g), and Fermi energy (E_f) in units of eV for WTe_2 monolayer system.

VBM (eV)	**CBM (eV)**	**E_g (eV)**	**E_f (eV)**
0.05	0.94	0.99	0.98

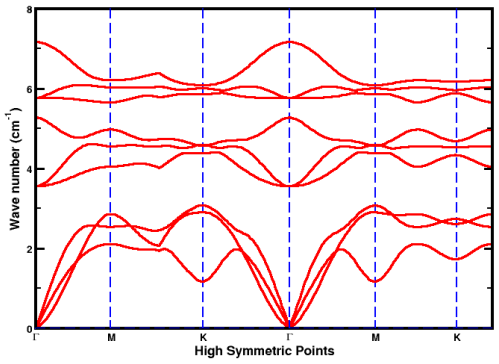

Figure 2: (Colour Online) phonon dispersion curves of WTe_2 compound, where frequency in term of wave numbers is plotted in y-axis and highly symmetric points are taken along the x-axis. Vertical dot lines touch the highly symmetric points.

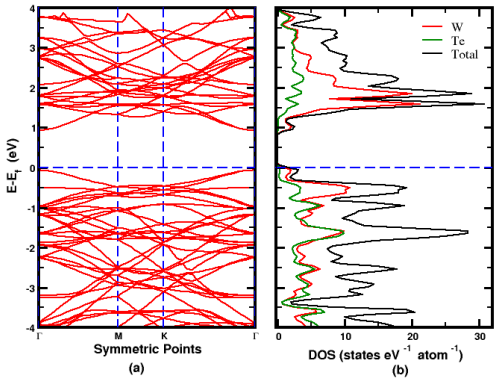

Figure 3: (Colour Online) (a) band structure of WTe_2 compound where high symmetric points are taken along the x-axis and corresponding energy are taken in y-axis. (b) density of states (DOS) plot of WTe_2 compound where energy of DOS states is taken along the y-axis and DOS states are taken along the x-axis. The horizontal dot line represents the Fermi energy level for both plots.

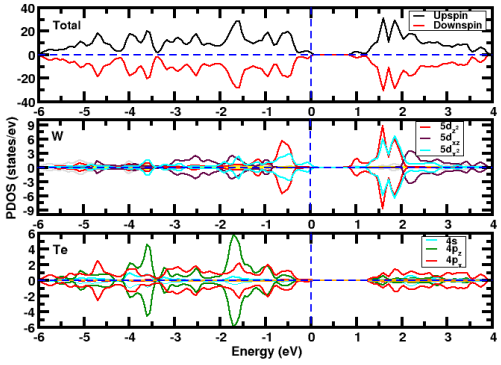

Figure 4: (Colour Online) partial density of states (PDOS) plot of WTe_2 compound, where horizontal dot lines separated the up and down spin states and vertical dot line distinguish the valance band region and conduction band region and is called fermi energy level.

Figure-3(b) represents the DOS plot of WTe_2 compound, where energy levels are plotted along y-axis and corresponding DOS states are plotted along x-axis. The blue dashed horizontal line at 0 eV separates the upper conduction band from the lower valence band. There is a gap between valence band and conduction band of value 0.91 eV. This verifies the findings from band structure. Near the immediate Fermi region, both in conduction and valence band, the DOS value is dominated due to W atoms. This suggests that near Fermi energy level greater quantum states that are available to be occupied are due to W atoms.

DOS and partial density of states (PDOS) calculations are used to explore the magnetic properties of material [37, 38]. PDOS is the measurement of DOS contributed by each sub-orbitals present in the material. Electrons with opposite spin couples and the magnetic moment becomes zero leading to non-magnetic nature. But, the presence of an unequal number of quantum states at a particular energy level, few electrons remain uncoupled contribute a non-zero magnetic moment which leads to magnetic properties. The PDOS plot of WTe_2 compound is shown in figure-4, where energy values of electronic states are plotted along x-axis and corresponding states are plotted along y-axis. The vertical blue dashed line at 0 eV represents the Fermi energy level situated at the boundary of the left valence band region and right conduction band region. The horizontal dot lines separate the distributed up-spin and down-spin states of electrons in the individual orbitals of atoms present in the material.

Tungsten (W) has electronic configuration [Xe] $4f^{14}$ $5d^4$ $6s^2$ where Xe represents Xenon atom and Tellurium (Te) atom is [Kr] $4d^{10}$ $5s^2$ $5p^4$. The contribution due to sub-orbitals present in valence shell has been plotted. The top plot is the total PDOS plot of considered material. The graph is symmetrical along the horizontal line; that suggests the presence of equal number of states available for both up-spin and down-spin electrons at a given energy level. Thus, the net magnetic moment of the system is zero and the material shows non-magnetic properties. The middle plot is the PDOS plot of W atoms. The d-orbitals in W atom has higher PDOS values as compare to its p and s-orbitals. The sub-orbital $5d_x{}^2$ has prominent values of PDOS states near the Fermi energy level whereas the sub-orbital $5d_z{}^2$ have dominant value of PDOS. It means, a greater number of unoccupied PDOS states are seen near the Fermi energy level. The bottom plot is the PDOS of Te atoms. In this case, p-orbitals have larger contribution for the production of magnetic moment. Near the Fermi energy level, PDOS states of $4p_z$ sub-orbitals have higher peaks than the PDOS states of s sub-orbitals. They reflect that there are a greater number of unoccupied orbitals are presented. The contribution of magnetic moment is due to the paring of up-and down-spins states. PDOS states of both W and Te atoms are symmetrical distributed around the Fermi energy level in the plots. Thus, it can be concluded that the net magnetic moment contributed by W and Te atoms have zero. Hence, the material shows non-magnetic properties.

3.4 Optical Properties

When a material is exposed to electromagnetic (EM) waves, many phenomena such as reflection, transmission, polarization of charges etc. are occurred [17]. A meticulous study of these phenomena can help to explore the potential usage of the materials in optoelectronics, energy storage, and sensing devices [26,39]. In this section, we discussed the optical properties of WTe_2 compound by the analysis of its dielectric function, optical conductivity, transmission, reflection and absorption coefficient. We have calculated dielectric tensor with the variation of photon energy in the range of 0 eV to 8 eV, for the study of material's dielectric function (constant). Dielectric tensor measures the dielectric constant in response to an applied electric field of material in a particular plane. The real and imaginary components of dielectric function are expressed by the relation: $\varepsilon(\omega) = \varepsilon_1(\omega) + i\varepsilon_2(\omega)$ [40].

Figures-5(a & b) are the imaginary and real dielectric function with respect to the photon energies plots of WTe_2 compound respectively, where dielectric function are taken along the y-axis and corresponding photon energy (eV) are taken in x-axis. These plots also show the variation of dielectric properties when an applied electric field is perpendicular (ε_{zz}) and parallel (ε_{xx}) and (ε_{yy}) to the plane of the material. Figure-5(b) shows the elements of the real part of the dielectric tensor, which indicate the degree of dipole polarization (and thus energy-storing capacity) caused by the applied electric field [41]. Polarization depends on the relative orientation of electric field to the plane of the material, where charges response due to the applied electric force. In 2D materials like monolayer WTe_2, there is a strong in-plane covalent bond with dense electron clouds. An applied electric field lies parallel to the plane, which caused the high polarization. Whereas in the case of between layers, two layers are bounded due to weaker van der Waal's force with less electron distribution. Hence, the applied electric field acted perpendicularly on the plane of material, which causes comparatively low polarization. That explained the higher value of ε_{xx} and ε_{yy} than ε_{zz} which are depicted in figure-5(b). At zero frequency, there is a finite static dielectric constant of magnitude 7.87 (of $\varepsilon_{xx} = \varepsilon_{yy}$) and 2.69 (of ε_{zz}) raised due to strong covalent bonding and van der Waals interaction. At lower frequencies of applied electric field, the charges can polarize effectively without any lag which gives the higher value of ε_{xx}, ε_{yy} and ε_{zz} in that frequency range. With the increase in frequency, charges with higher masses lag to polarize and thus resulting in a decreased polarization. It explains the decreasing value of dielectric function, and hence ε_{zz} becomes zero at 4.65 eV. The ε_{xx} and ε_{yy} of real dielectric functions become zero at 3.47 eV while ε_{xx} and ε_{yy} of imaginary dielectric functions show peaks at 3.47 eV. At that energy, the charge oscillators resonated with the applied electric field, and leading to no net polarization. Hence, real dielectric function plots equal to zero. That phenomenon results maximum energy absorption. In the negative region, the material does not store energy. At higher energies, ε_1 reached to zero which is due to rapid response of electron for the oscillation of electric field. It signifies that monolayer WTe_2 becomes transparent to high energy photons. Similar results are obtained in previous computational and experimental studies of other TMDCs materials [42]. These unique properties of WTe_2 can be exploited in photonic and energy storage devices.

The imaginary part of the dielectric function ε_2 in figure-5(a) represents the energy loss (or absorption) of photons due to lagging response of electrons to the electric field (or inter-band transitions) [43]. The imaginary part of dielectric function also showed anisotropic properties. In layer, strong covalent bonding and denser electron cloud results greater energy loss and absorption than that of the out-plane region. It explained the higher value of $\varepsilon_{xx} = \varepsilon_{yy}$ than ε_{zz}. The dielectric constant rises from zero to maximum value with several peaks and dips gradually falling back to zero with the increasing photon energy values of material. In the energy range below the band gap energy (0.99 eV) value, the dielectric function is determined to be zero. It is signifying that there are no excitonic transitions [44], and hence electrons polarize well in response to the slow changing electric field without any lag. When the energy of photons increased beyond 0.99 eV, the energy becomes sufficient for electronic transitions from valence band to conduction band. That explains the sudden increases the graph after energy more than band gap energy. At energy 2.05 eV, distinct peaks can be seen in the graph which showing the absorption of energy due to inter-band electronic transition. A dip region can be seen at energy 2.71 eV, representing the electron unavailability of transition states around this energy range. It could be explained by the change the electronic structure of material. The peaks at 4.65 eV of ε_{zz}, at 3.47 eV of ε_{xx} and ε_{yy} are obtained due to energy loss caused by resonance of charged oscillators and electric field. The material became transparent in increasing value of photon energy because there is not transition of photon in the region. This means, no energy loss occurred as a result the graph approaches to a zero value is shown in figure-5. Our obtained results are liked similar with the results obtained by others authors in the reported literature [45].

When light interacts with electrons in a substance, an oscillating electric field is created, which explains optical conductivity. The induced cur-

rent density J(ω) is given due to the oscillating electric field which is calculated as the product of optical conductivity $\sigma(\omega)$ and the applied electric field E(ω). It is expressed by the relation: J(ω)=$\sigma(\omega)\varepsilon(\omega)$, where ω is the angular frequency of the applied field . Studying optical conductivity is crucial to understanding how well a material can conduct electricity or release energy when exposed to light. Optical conductivity is also a complex quantity that is $\sigma\ (\omega)=\sigma^{'}(\omega)+i\sigma^{''}(\omega)$, where $\sigma^{'}(\omega)$ is the real part measuring energy loss due to absorption and $\sigma^{''}(\omega)$) is imaginary part measuring reactive components relating to energy storage and phase shift [22]. In the present work, we have calculated the optical conductivity of WTe_2 monolayer material. The real part of optical conductivity is related to the imaginary part of dielectric function. These two quantities are related by Maxwell's equation [23], $\sigma^{'}(\omega)=\omega\ \varepsilon_0\ \varepsilon_2(\omega)$. where ε_0 is the permittivity of free space. Thus, the plot of these two quantities is similar evident from figure-5(a) and figure-5(d). In figure-5(d), the real optical conductivity is plotted against increasing energy of light. Below 0.99 eV (i.e. band gap energy value), the graph is flat and equal to zero. It suggests no electric current, hence absence of excitonic states. But, as the energy is increased above band gap energy value, the graph sharply increased. It represents the increasing conductivity. A sharp peak in graph at 2.05 eV is due to increase conductivity caused by inter-band electronic transition. An increased conductivity can be seen within the range 3 eV to 4 eV which is due to resonance of electrons with the electric field. Conductivity is unaffected by additional light energy because electronic transitions are uncommon at this level.

The imaginary optical conductivity $\sigma_2(\omega)$ is related to the real part of dielectric function. Figure-5(c) shows the variation of imaginary optical conductivity (plotted along y-axis) with the increasing photon energy (plotted along x-axis). As the photon energy increases, the value of $\sigma_2(\omega)$ decreases gradually below zero and makes a peak at 1.82 eV photon energy. Further increasing the photon energy results in an increase in the curve below zero, and the curve touches the zero level at energy 3.32 eV. Beyond this, the graph increases in the positive region making peaks and dips representing the intensity of polarization in the material.

Additionally, we have discussed about the absorption, reflection and transmission coefficient a material through the analysis of its photon energy plots which are shown in figure-6(a-c) respectively.

At lower frequency (below band gap energy 0.99 eV), the absorption coefficient is reached zero as shown in figure-6(a). It suggests that there is no energy loss and inter-band electronic transition because there is only occurred excitonic transitions. Hence, zero absorptance is possible below the energy of 0.99 eV. Phonon assisted transition and inter-band electronic transition in the region of photon energy greater than 0.99 eV. Thus, the absorption curve increases with increase the frequency having certain peaks. They are representing electronic transitions from valence band to conduction band. At energy 2.10 eV, a significant peak can be observed in absorption curve which is due to inter-band transition of electrons. A significant absorption of energy can be seen within the energy range 3 eV to 4 eV because in that region greater amount of energy loss of a material due to the resonance of electrons. Beyond 4 eV photon energy, the absorption curve gradually decreases to zero because at higher energy inter-band transitions become unlikely and the materials become transparent.

Transmission coefficient of material is explored by carefully interpretation by the variation of transmission coefficient with the values of photon energy, which is shown in figure-6(b). Transmission curve is symmetrical and inversely related to both absorption and reflection coefficient curves. The absorption or reflection curves are increased due to the decrease the value of transmission coefficient of a material and vice versa. It is also found that 100% transmissivity of material is seen below the value of photon energy 0.99 eV. This is due to no interaction between electrons and photons for inter-band electronic transition. But, energy of the photon is increased, the inter-band electronic transitions are occurred, and transmissivity of the material decreases which are illustrated in figure-6(b). decreasing the transmission coefficient of a material is due to existence of inter-band transition and resonance of electrons at 2.10 eV, and within (3-4) eV energy range respectively. The energy of photon is further increased beyond 4 eV, which reflects that there will be less value of reflection coefficient of a considered material.

Reflectivity represents the fraction of incident light that gets reflected from the surface of a material [31–33]. The figure-6(c) represents the variability of reflectivity of the material against the energy of the incident photons. Below the photon energy 0.99 eV, the reflection curve is horizontal and equal to zero. It indicates, no reflection of incident photons. The reflection curve suddenly raised with increase of its photon energy because of increasing the interaction between photons and electrons. Different peaks of reflection coefficient are seen at 1.99 eV and in between (3-4) eV photon energy. They happened as a result of a severe electron transition that caused a large amount of photon reflection. But, at high energy region, reflection coefficient approaches to zero value of photon energy which, indicates the decreasing the reflectivity.

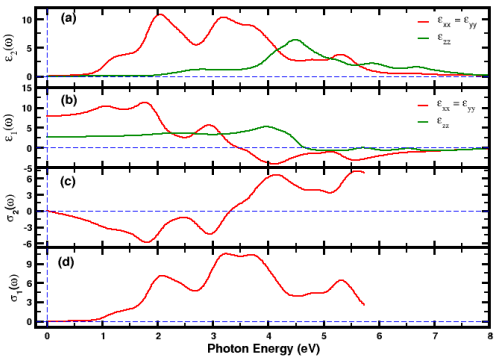

Figure 5: (Colour Online) plots of dielectric function and optical conductivity with phonon energies, (a) imaginary part of dielectric function, (b) real part of dielectric function, (c) imaginary optical conductivity, and (d) real part of optical conductivity. All of these graphs are plotted against photon energy (eV).

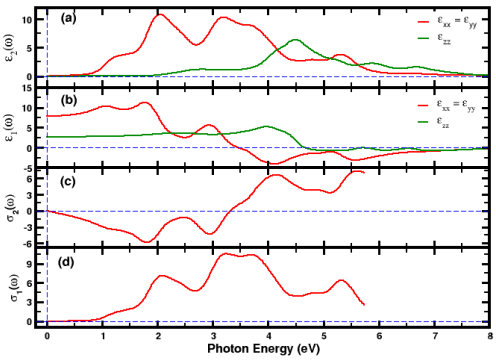

Figure 6: (Colour Online) graph between photon energies with absorption, transmission and reflection coefficient, (a) Absorption coefficient with photon energy, (b) Transmission coefficient with photon energy, and (c) Reflection coefficient with photon energy.

4 Conclusions

In this work, we explored the structural, electrical, magnetic, mechanical, dynamical, thermal, and optical characteristics of a WTe_2 monolayer supercell structure computationally by using density functional theory (DFT) technique. We found that WTe_2 compound is structurally, and dynamically stable p-type semiconductor. From the interpretation of material's density of states and partial density of states plots, it was found that up-and down-spins states of electron in the orbitals of atoms are symmetrically distributed around the Fermi energy level, and hence WTe_2 monolayer supercell structure has non-magnetic properties. Mechanical properties of a considered material are studied by calculating the parameters like modulus of rigidities, elastic constants, compressibility, and anisotropy factor. The material is found to be ductile and anisotropic in nature. Furthermore, thermal properties of a material are examined by calculating material's phonon velocity and Debye temperature. The longitudinal, transverse, average phonon velocities and Debye temperature of considered material are found to be 1665.76m/s, 971.05 m/s, 1077.12 m/s and 85.6K respectively. Hence, WTe_2 is a low melting point material. Additionally, optical properties of WTe_2 compound are predicted through its dielectric function, optical conductivity, absorption coefficient, transmission coefficient, and reflection coefficient. At high photon energy region, WTe_2 has been more transparent, anisotropic nature, increasing conductivity, small values of absorption and reflection coefficients. Hence, it can be used in the fields of optoelectronic and energy storage devices.

Acknowledgement

The authors would like to acknowledge the condensed matter research lab CDP TU, TWAS research funds RG 20-316, network project NT-14 of ICTP/OE for the computing capacity, and Prof. NP Adhikari for his excellent input on the manuscript.

Author Contributions

SKY, TN, AP, KK, KD and OSR generated the data and wrote the manuscript using formal data analysis. HKN came up with the idea, managed the project, analyzed the information, and revised and assessed the text.

Declarations Conflict of Interests

The authors certify that none of the work contained in this paper may be influenced by any known conflicts of interest, either financial or personal.

References

[1] K. S. Novoselov, D. Jiang, F. Schedin, T. J. Booth, V. V. Khotkevich, S. V. Morozov, and A. K. Geim. Two-dimensional atomic crystals. *Proceedings of the National Academy of Sciences*, 102(30):10451–10453, 2005.

[2] Y. Xiao, W. Zheng, B. Yuan, C. Wen, and M. Lanza. Highly accurate thickness determination of 2d materials. *Crystal Research and Technology*, 56(6):2100056, 2021.

[3] M. Xu, T. Liang, M. Shi, and H. Chen. Graphene-like two-dimensional materials. *Chemical reviews*, 113(5):3766–3798, 2013.

[4] J. A. Wilson and A. D. Yoffe. The transition metal dichalcogenides discussion and interpretation of the observed optical, electrical and structural properties. *Advances in Physics*, 18(73):193–335, 1969.

[5] K. Zhang, Y. Feng, F. Wang, Z. Yang, and J. Wang. Two-dimensional hexagonal boron nitride (2d-hbn): synthesis, properties and applications. *Journal of Materials Chemistry C*, 5(46):11992–12022, 2017.

[6] S. Manzeli, D. Ovchinnikov, D. Pasquier, O. V. Yazyev, and A. Kis. 2d transition metal dichalcogenides. *Nature Reviews Materials*, 2(8):1–15, 2017.

[7] A. Kuc, T. Heine, and A. Kis. Electronic properties of transition-metal dichalcogenides. *MRS Bulletin*, 40(7):577–584, 2015.

[8] K. S. Novoselov, A. Mishchenko, A. Carvalho, and A. H. Castro Neto. 2d materials and van der waals heterostructures. *Science*, 353(6298):aac9439, 2016.

[9] R. J. Toh, Z. Sofer, and M. Pumera. Catalytic properties of group 4 transition metal dichalcogenides (mx 2; m= ti, zr, hf; x= s, se, te). *Journal of Materials Chemistry A*, 4(47):18322–18334, 2016.

[10] A. Splendiani, L. Sun, Y. Zhang, T. Li, J. Kim, C. Y. Chim, and F. Wang. Emerging photoluminescence in monolayer mos2. *Nano Letters*, 10(4):1271–1275, 2010.

[11] A. Raza, U. Qumar, J. Hassan, M. Ikram, A. Ul-Hamid, J. Haider, et al. A comparative study of dirac 2d materials, tmdcs and 2d insulators with regard to their structures and photocatalytic/sonophotocatalytic behavior. *Applied Nanoscience*, 10:3875–3899, 2020.

[12] D. Xiao, G. B. Liu, W. Feng, X. Xu, and W. Yao. Coupled spin and valley physics in monolayers of mos 2 and other group-vi dichalcogenides. *Physical review letters*, 108(19):196802, 2012.

[13] A. K. Singh, P. Kumar, D. J. Late, A. Kumar, S. Patel, and J. Singh. 2d layered transition metal dichalcogenides (mos2): synthesis, applications and theoretical aspects. *Applied Materials Today*, 13:242–270, 2018.

[14] K. F. Mak and J. Shan. Photonics and optoelectronics of 2d semiconductor transition metal dichalcogenides. *Nature Photonics*, 10(4):216–226, 2016.

[15] H. K. Neupane and N. P. Adhikari. Tuning structural, electronic, and magnetic properties of c sites vacancy defects in graphene/mos2 van der waals heterostructure materials: A first-principles study. *Advances in Condensed Matter Physics*, 2020(1):8850701, 2020.

[16] H. K. Neupane and N. P. Adhikari. Effect of vacancy defects in 2d vdw graphene/h-bn heterostructure: First-principles study. *AIP Advances*, 11(8), 2021.

[17] P. Giannozzi, S. Baroni, N. Bonini, M. Calandra, R. Car, C. Cavazzoni, et al. Quantum espresso: a modular and open-source software project for quantum simulations of materials. *Journal of physics: Condensed Matter*, 21(39):395502, 2009.

[18] P. Hohenberg and W. Kohn. Inhomogeneous electron gas. *Physical Review*, 136(3B):B864, 1964.

[19] W. Kohn and L. J. Sham. Self-consistent equations including exchange and correlation effects. *Physical Review*, 140(4A):A1133, 1965.

[20] B. G. Pfrommer, M. Cote, S. G. Louie, and M. L. Cohen. Relaxation of crystals with the quasi-newton method. *J. Comput. Phys.*, 131(1):233–240, 1997.

[21] D. H. Chung and W. R. Buessem. The voigt-reuss-hill approximation and elastic moduli of polycrystalline mgo, caf2, β-zns, znse, and cdte. *Journal of Applied Physics*, 38(6):2535–2540, 1967.

[22] A. Togo and I. Tanaka. First principles phonon calculations in materials science. *Scripta Materialia*, 108:1–5, 2015.

[23] W. Körner and C. Elsässer. First-principles density functional study of dopant elements at grain boundaries in zno. *Physical Review B—Condensed Matter and Materials Physics*, 81(8):085324, 2010.

[24] E. Torun, H. Sahin, S. Cahangirov, A. Rubio, and F. M. Peeters. Anisotropic electronic, mechanical, and optical properties of monolayer wte2. *Journal of Applied Physics*, 119(7):074307, 2016.

[25] W. Voigt. *Lehrbuch der Kristallphysik (Textbook of crystal physics)*. BG Teubner, Leipzig und Berlin, 1928.

[26] B. A. Reu. Berechnung der fließgrenze von mischkristallen auf grund der plastizitätsbedingung für einkristalle. *ZAMM-Journal of Applied Mathematics and Mechanics/Zeitschrift für Angewandte Mathematik und Mechanik*, 9(1):49–58, 1929.

[27] R. Hill. The elastic behaviors of a crystalline aggregate. *Proceedings of the Physical Society. Section A*, 65(5):349, 1952.

[28] H. Fu. Anisotropy affects the lattice waves and phonon distributions in gaas. *The European Physical Journal B*, 93(10):199, 2020.

[29] M. L. Cohen. Calculation of bulk moduli of diamond and zinc-blende solids. *Physical Review B*, 32(12):7988, 1985.

[30] Z. Chen, U. Gandhi, J. Lee, and R. H. Wagoner. Variation and consistency of young's modulus in steel. *Journal of Materials Processing Technology*, 227:227–243, 2016.

[31] O. S. Rijal, H. K. Neupane, D. Oli, R. K. Neupane, P. Shrestha, S. Sharma, et al. A first-principles investigation of the structural, mechanical, dynamic, electronic, magnetic, and optical properties of ti2ac (a= cd, s) max phase compounds. *Journal of Physics D: Applied Physics*, 58(12):125102, 2025.

[32] D. Oli, H. K. Neupane, R. K. Neupane, O. S. Rijal, P. Shrestha, S. Sharma, et al. Comprehensive study of structural, mechanical, dynamical, electronic, magnetic, and optical properties of ti3gec2 and ti3sic2 compounds via dft approach. *Physica B: Condensed Matter*, page 417009, 2025.

[33] H. K. Neupane, D. Oli, O. S. Rijal, R. K. Neupane, P. Shrestha, S. Sharma, et al. Exploring the structural, dynamical, mechanical, electronic, magnetic, and optical properties of ta2aln, ti2aln & ti2gan max phase compounds: First-principles study. *Heliyon*, 2025.

[34] R. Qi, R. Shi, Y. Li, Y. Sun, M. Wu, N. Li, et al. Measuring phonon dispersion at an interface. *Nature*, 599(7885):399–403, 2021.

[35] P. Lu, J. S. Kim, J. Yang, H. Gao, J. Wu, D. Shao, et al. Origin of superconductivity in the weyl semimetal wt e 2 under pressure. *Physical Review B*, 94(22):224512, 2016.

[36] Z. Xu, B. Luo, Z. B. Siu, Y. Chen, J. Huang, Y. Li, et al. Phonon spectrum and electronic structures of wte2: A first-principles calculation. *Physics Letters A*, 389:127081, 2021.

[37] H. K. Neupane and N. P. Adhikari. Adsorption of water molecule in graphene/mos2 heterostructure with vacancy defects in mo sites. *Advances in Condensed Matter Physics*, 2022(1):2135213, 2022.

[38] H. K. Neupane and N. P. Adhikari. Structure, electronic and magnetic properties of 2d graphene-molybdenum disulphide (g-mos2) heterostructure (hs) with vacancy defects at mo sites. *Computational Condensed Matter*, 24:e00489, 2020.

[39] G. Q. Huang. Dynamical stability and superconductivity of li-intercalated bilayer mos2: A first-principles prediction. *Phys. Rev. B*, 93(10):104511, 2016.

[40] Y. Wu, X. Wang, Y. Wang, Y. Duan, and M. Peng. Insights into electronic and optical properties of agds2 (a= li, na, k, rb and cs) ternary gadolinium sulfides. *Optical Materials*, 114:110963, 2021.

[41] J. G. Kirkwood. On the theory of dielectric polarization. *The Journal of Chemical Physics*, 4(9):592–601, 1936.

[42] A. Kumar and P. Ahluwalia. Electronic structure of transition metal dichalcogenides monolayers 1h-mx2 (m= mo, w; x= s, se, te) from ab-initio theory: new direct band gap semiconductors. *The European Physical Journal B*, 85(1):1–7, 2012.

[43] M. Davies. Dielectric absorption. *Quarterly Reviews, Chemical Society*, 8(3):250–278, 1954.

[44] B. Sun, W. Zhao, T. Palomaki, Z. Fei, E. Runburg, P. Malinowski, et al. Evidence for equilibrium exciton condensation in monolayer wte2. *Nature Physics*, 18(1):94–99, 2022.

[45] J. Pešić, J. Vujin, T. Tomašević-Ilić, M. Spasenović, and R. Gajić. Dft study of optical properties of mos2 and ws2 compared to spectroscopic results on liquid phase exfoliated nanoflakes. *Optical and Quantum Electronics*, 50(7):291, 2018.